

Lasers in Manufacturing Conference 2019

Effects of titanium on grain boundary strength in the molybdenum laser weld bead zone and formation and strengthening mechanisms of parasitic brazing layers

Liang-Liang Zhang^a, Lin-Jie Zhang^{a*}, Jian Long^a, Jie Ning^a, Jian-Xun Zhang^a,
Suck-Joo Na^{a,b}

^aState key laboratory of mechanical behavior for materials, Xi'an Jiaotong University, Xi'an, 710049, China

^bDepartment of Mechanical Engineering, KAIST, 291 Daehak-ro, Yuseong-gu, Daejeon 305-701, Republic of Korea

Abstract

Molybdenum (Mo) has tremendous application potential in the nuclear power field, but its application is limited by the grain-boundary embrittlement of fusion-welded joints made of it. In this study, titanium (Ti) was selected as an alloying element to reduce the brittleness of laser weld beads in Mo "cladding-end plug" socket joints. Parasitic brazing was also performed to enhance the joint strength. Joints with the same strength as the base material and a hydraulic bursting pressure of 60 MPa were produced using a combination of the two methods. The analysis indicates the following. After being added to the welded zone, Ti was able to combine with the free oxygen (O), forming TiO₂ and at the same time reducing the MoO₂ content of the grain surface. O and MoO₂ are both the main causes of the embrittlement of Mo grain boundaries. In addition, by taking advantage of the high melting point and thermal conductivity of Mo, a Ti foil pre-placed between the Mo tube and rod in the socket joint was melted, forming metallurgical bonding, which further improved the bearing capacity of the joint. These results could facilitate the application of Mo in the nuclear power field and also provide a new approach for improving the performance of socket joints made of refractory materials.

Keywords: molybdenum; titanium; laser beam welding; grain boundary embrittlement; brazing

1. Introduction

Molybdenum (Mo) alloys are one of the main candidate materials for producing accident-tolerant fuel cladding for next-generation nuclear power stations. However, the embrittlement of the Mo alloy welded joints significantly limits their engineering applications. There are two main causes of the embrittlement of Mo: (1) intrinsic intergranular brittleness [1, 2] and (2) extrinsic brittleness caused by the segregation of impurity elements at the grain boundaries [3-6], of which oxygen (O) has the most significant impact [7]. As a result of these factors, the strength of a Mo welded joint is generally only 30–50% of that of the base material (Table 1).

There are two main methods for improving the bonding strength of Mo grain boundaries. (1) Reducing the interfacial energy. For example, low-angle grain boundaries and coincidence site lattice

* Corresponding author. Tel.: 86-29-82663115; Fax: 86-29-82663115
E-mail: zhanglinjie@mail.xjtu.edu.cn (L-J Zhang)

(CSL) grain boundaries with a low Σ value (the volumetric ratio of unit cells of the CSL to those of the actual lattice) have relatively low interfacial energies [2]. (2) Reducing the extrinsic brittleness by microalloying. According to the different strengthening mechanisms on the Mo grain boundary, elements are divided into two categories, ① those that can directly strengthen Mo grain boundaries (e.g., boron (B) [3, 4, 6], carbon (C) [3, 4, 6, 8], titanium (Ti) [9] and rhenium (Re) [10]) and ② those that cannot directly strengthen Mo grain boundaries but can stimulate Mo grain boundary-strengthening elements (e.g., B and C) to accumulate at Mo grain boundaries, prevent Mo grain boundary-weakening elements (e.g., O and nitrogen (N)) from segregation at Mo grain boundaries, or compete for the sites of O and N at the Mo grain boundaries (e.g., hafnium (Hf) [11, 12], zirconium (Zr) [13, 14] and nickel (Ni)). Of the category ① elements, B, C and Ti are prone to form oxides with the O in Mo, thereby reducing the free O content [13]. The selection of alloying elements for the fusion welding of Mo generally should meet the following criteria:

- no brittle phase is formed, and the element is highly metallurgically compatible with Mo;
- they have no significant impact on the performance of Mo at high temperatures and in irradiation environments;
- the alloying process is easy to implement.

Carburization is the main method for using C to alloy Mo. Carburization requires a high temperature (1,200–1,500 °C) [15, 16] and has a complex process and high manufacturing costs. Re (20–50wt%) can significantly improve the toughness of Mo [10, 17] but reduces its resistance to neutron irradiation [18]. Re also has extremely low reserves globally and is very costly. B and Hf are unable to considerably increase the strength of Mo [11, 12]. Zr is prone to the formation of a brittle Mo₂Zr phase [19] with Mo and can also increase the ductile-brittle transition temperature [13, 14]. Ni can easily form an approximately 2-nm δ Ni layer on the Mo grain-boundary surface, thereby reducing the grain-boundary strength [20]. Considering the deficiencies in the above mentioned elements and based on the selection criteria for alloying elements introduced in the previous paragraph, Ti is found to have notable advantages. First, no brittle phase is formed when mixing Ti and Mo (Fig. 1); Ti and Mo are infinitely miscible in one another at high temperatures. Second, Ti can easily combine with O [15, 21], thereby reducing the content of free O in Mo. Moreover, because the solidification temperature of Ti (1,670 °C [22]) is far lower than that of Mo (2,623 °C [22]), Ti is prone to crystallization at the Mo grain boundaries and form dispersive, fine TiO₂ particles with the O at the Mo grain boundaries [23]. TiO₂ particles can prevent grain-boundary migration during the deformation process [14, 24, 25]. Hence, Ti is selected in this study as the microalloying element for Mo laser welded joints.

Considering the relatively high melting point (2,623 °C [22]) and high thermal conductivity (138 W/m·K (MatWeb database)) of Mo and based on the unique socket structure of cladding-end plug joints, a low-melting point (1,670 °C [22]) Ti foil was pre-placed in the tube-rod overlap zone, and brazing between the tube and rod in the heat-affected zone (HAZ) was achieved by welding thermal cycling to further strengthen the joint.

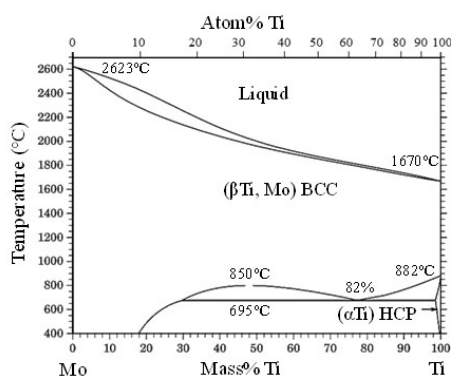


Fig. 1. Mo-Ti binary alloy phase diagram [22]

2. Materials and methods

2.1. Materials

A lanthanum oxide (La_2O_3) dispersion-strengthened Mo alloy (La content: ca. 0.25wt%) provided by Jindulicheng Molybdenum Group Co., Ltd. was used in this study. Cladding tubes and solid end plugs were produced by forging and hot rolling. Fig. 2(a) shows the shape and dimensions of the cladding tubes and solid end plugs.

2.2. Laser welding system

The laser welding system consists of an IPG TLS-4000 optical fibre laser device, a Yaskawa HP20 robot, a rotary fixture, a preheating device and an argon (Ar) shielding device, as shown in Fig. 2(b). The laser device has a maximum output power of 4 kW and a wavelength of 1,070 nm. Ar with a purity of 99.999% was used in the experiment.

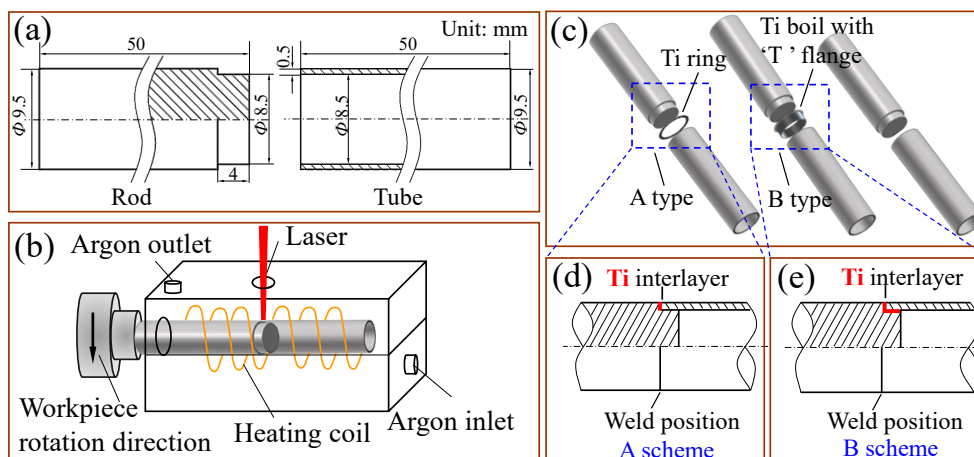


Fig. 2. (a) Schematic diagram of the laser welding system; (b) structure and dimension of a workpiece; (c) schematic diagram of the alloying of a Mo rod-Mo tube socket joint; (d) method A for adding Ti foil (Ti foil is pre-placed in the weld zone; no Ti foil is pre-placed in the overlap zone); (e) method B for adding Ti foil (Ti foil is pre-placed in both the weld and overlap zones)

2.3. Micro-alloying by Ti element

TA1 Ti foil sheets (Ti content: 99.99wt%) with thicknesses of 0.03, 0.06 and 0.09 mm were used in the micro-alloying of the Mo alloy laser welded joints. Prior to the welding, the Mo rods and tubes were polished using sandpaper and cleaned with acetone to remove the oxide films and oil stains on their surfaces. Welding was completed within 20 min after the polishing and cleaning procedures were completed. In the experiment, Ti was added using two different methods, A and B. (1) Method A: Ti foil

was added in a circular form (Fig. 2(d)). (2) Method B: Ti foil was added in a "T-flange"-shaped form (Fig. 2(e)). Two sets of experiments were conducted to analyse the effect of the Ti and the method of addition on the joint performance (Table 2). In the following sections, each Ti-alloyed joint is denoted by Mo-xTi-A/B (x represents the thickness of the Ti foil, and A/B represents the method of addition). The non-alloyed joint is denoted by pure Mo.

Table 1. The experimental parameters of Mo laser welding with Ti element

Test No.	Designation of joint	Ti foil thickness (mm)	Ti addition scheme	Preheating temperature (°C)	Defocus amount (mm)	Welding speed (m/min)	Laser power
No. 1	Mo-0.03Ti-A	0.03	A	450	2	2	1.2 kW
	Mo-0.06Ti-A	0.06	A	450			
	Mo-0.09Ti-A	0.09	A	450			
No. 2	Mo-0.03Ti-B	0.03	B	450			

2.4. Mechanical testing and microstructure analysis

A mixture of a 10% sodium hydroxide solution and a 10% potassium ferricyanide(III) solution (1:1, v:v) was used as the etching solution to etch each metallographic specimen for 30 s. Electron backscatter diffraction (EBSD) specimens were prepared by electropolishing in a mixture of sulfuric acid and ethanol (1:7, v:v) for 2–5 s under a voltage of 18 V and a current of 0.6 A. An Oxford EBSD system was used to conduct the EBSD analysis. Transmission electron microscope (TEM) specimens were prepared by successively grinding using silicon carbide sandpaper with grit sizes of 500–3,000 to a thickness of approximately 30 μm and then ultimately thinning by twin-jet electropolishing with a 10% nital solution.

Each socket joint was subjected to a tensile test on an Instron 1195 tensile testing machine at a rate of 0.1 mm/min. A Zeiss Gemini 500 scanning electron microscope (SEM) was used to observe the morphology of the tensile fractures. In addition, an Oxford energy dispersive spectroscopy (EDS) system equipped with SEM was used to determine the composition of the precipitated phase on the surface. A JEM-2100Plus high-resolution scanning-transmission electron microscope (STEM) was used to analyse the precipitated phase under an accelerating voltage of 200 kV. A hydraulic bursting test was performed on each joint until failure, during which the pressure was increased at a rate of 4.3 MPa/min. A hydrostatic test was also performed, during which the pressure was increased up to 21 MPa at a rate of 1.05 MPa/min.

A Thermo Fisher ESCALAB Xi+ X-ray photoelectron spectrometer (XPS) was used to analyse the grain-boundary surface in the welded zone. The testing conditions are summarized as follows: beam spot size: 100 μm ; analyser mode: pass energy 20.0 eV; radiation source: Al-K α ; and step size: 0.05 eV. The spectral peaks were calibrated using the binding energy of C 1s (284.6 eV). To prevent oxidation, each specimen was placed in the vacuum chamber of the XPS immediately after tensile failure, and its grain-boundary surface was cleaned using 1,000-eV Ar ions for 30 s.

A JXA8100 electron probe microanalyzer (EPMA) was used to determine the composition of the welded zone and the brazing layer of each specimen that had been previously cleaned ultrasonically in acetone for 30 min.

3. Results

3.1. Mechanical properties and microstructure of the weld bead

First, to determine the content and distribution of Ti in each joint, the Mo-0.09Ti-A joint (the joint with the highest Ti content) was subjected to cross-sectional analysis. The EPMA analysis shows that the weld bead (WB) of the Mo-0.09Ti-A joint contained a Ti content of 2.08wt% on average. The EDS surface scanning of the Mo-0.09Ti-A joint (Fig. 3(b)) shows that Ti was evenly distributed in the whole welded zone. A notable sudden change can be observed on the EDS line-scanning curve of Ti at the HAZ-welded zone interface.

Second, the tensile test results for the joints showed that the strength of each joint increased significantly after Ti was added into the WB (Fig. 4). The maximum strength of the Mo-0.03Ti-A joint reached 455 MPa, which was 64.5% of the strength of the base material. By contrast, the strength of the

pure Mo joint (229.8 MPa) was only 32.5% of that of the base material. The fracture occurred in the welded zone of each of these two joints. The maximum tensile strength of the joint was 455, 450 and 385 MPa when a Ti foil sheet with a thickness of 0.03, 0.06 and 0.09 mm was added, respectively. The addition of Ti resulted in a decrease in the width of the welded zone, an increase in the depth of the welded zone and the formation of some fine-grained zones (FGZs). The higher the Ti content, the narrower and deeper the welded zone (Fig. 5(a)), and the smaller the grains in the FGZs (Fig. 5(b)). The appearance of the fine-grained area may be related to the constitutional supercooling during the solidification of the molten pool [32] and the behaviour of the keyhole [33, 34]. An EBSD system was used to analyse the types of grain boundaries on the cross-section of the pure Mo and Mo-0.03Ti-A joints. The addition of Ti resulted in an increase in the number of low- Σ value CSL grain boundaries (Fig. 5(c) and (d)), i.e., an increase in the number of grain boundaries with relatively high strength [2, 35, 36].

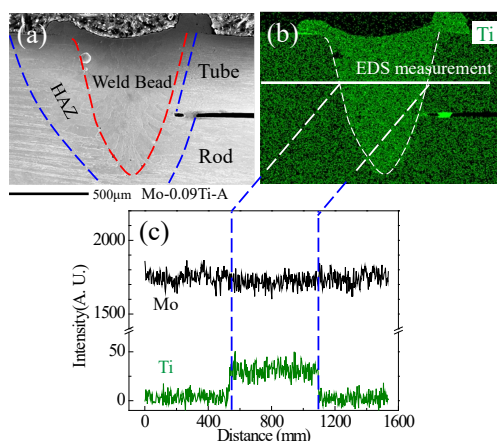


Fig. 3. SEM and compositional analysis of the cross-section of the Mo-0.09Ti-A joint: (a) SEM image; (b) EDS area scan image; (c) EDS line scan image

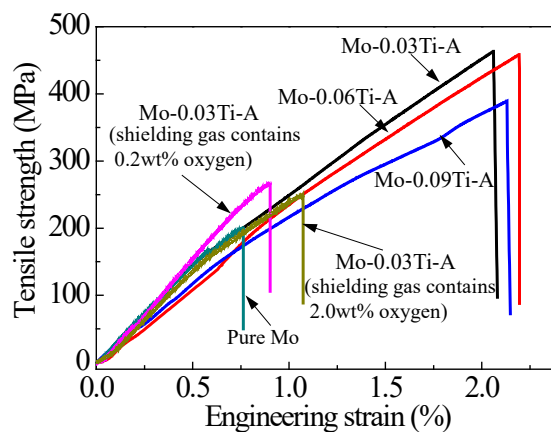


Fig. 4. Tensile strength-displacement curves of the Mo tube-Mo rod socket joints

The fractures of the pure Mo joint and the Mo-0.03Ti-A joint (the joint with the highest strength) were further observed under the SEM (Fig. 6(a) and (c)). First, an intergranular fracture was observed in each of the two joints. Second, a sheet-like and conical precipitated phase (the white phase in Fig. 6(a)) was found to be distributed on the grain-boundary surface in the welded zone of the pure Mo joint, and its O content (P1 and P2 in Table 3) was higher than that at other sites of the fracture (P3 and P4 in Table 3). The TEM diffraction pattern of this phase (Fig. 6(b)) was indexed as MoO₂. The second phase distributed on the grain-boundary surface in the welded zone of the Mo-0.03Ti-A joint (the joint with the highest strength) consisted of circular particles of diameter generally greater than 10 nm but less than 20 nm (Fig. 6(c)). These particles contained a relatively high Ti content (P5, P6, P7 and P8 in Table 3). The TEM diffraction pattern of this phase (Fig. 6(d)) was indexed as TiO₂.

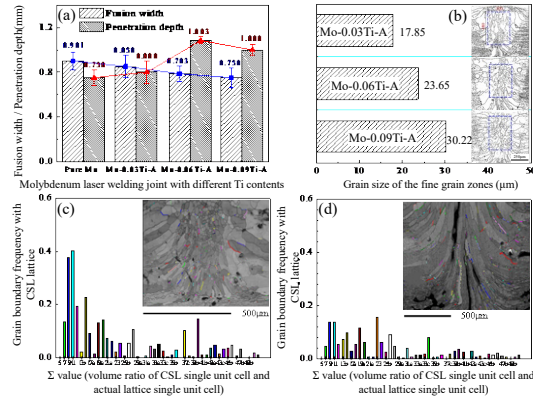


Fig. 5. (a) Depth and width of the welded zone; (b) average grain size in the FGZs in the welded zone after alloying with Ti; (c) statistical EBSD results for CSL grain boundaries in the welded zone of the pure Mo joint; (d) statistical EBSD results for CSL grain boundaries in the welded zone of the Mo-0.03Ti-A joint.

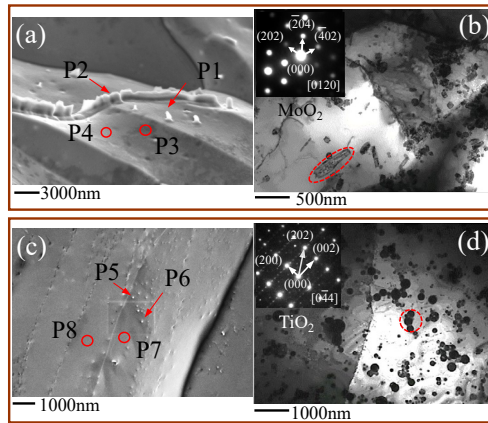


Fig. 6. (a) SEM image of the fracture of the pure Mo joint; (b) TEM bright field image of the weld bead zone of the pure Mo joint; (c) SEM image of the fracture of the Mo-0.03Ti-A joint; (d) TEM bright-field image of the weld bead zone of the Mo-0.03Ti-A joint.

Finally, the strength of the joints obtained by adding Ti foil using the two different methods (A and B) was comparatively analysed. The results showed the following. The maximum tensile strength of the Mo-0.03Ti-B joint was as high as 690 MPa (Fig. 7(a)), and the fracture occurred in the base material on the Mo tube side (Fig. 7(b)). No leak occurred during the hydrostatic test on the socket joint when the pressure increased from 0 to 21 MPa. During the hydraulic bursting test, the bursting pressure reached 60 MPa (Fig. 7(c) and (d)); the nuclear fuel cladding tube in a pressurized water reactor is generally under a pressure of 15.5 MPa [37], which is one-fourth of the bursting pressure that was obtained during the hydraulic bursting test.

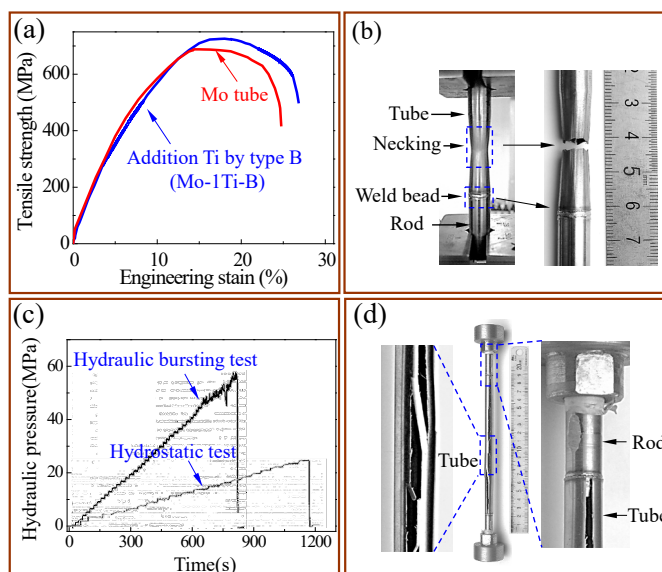


Fig. 7. (a) Strength-displacement curves of Mo-0.03Ti-B and pure Mo tube; (b) images of the joint after fracture testing; (c) hydrostatic test curve and hydraulic bursting test curve for the molybdenum joint of Mo-0.03Ti-B; (d) images of joint after hydraulic bursting testing

4. Discussion

A decrease in the strength of Mo grain boundaries is generally believed to be caused by O precipitation and the formation of the product of its combination with Mo, MoO_2 [1, 3, 7] and large amount of MoO_2 were found on the grain boundary of pure Mo joint. But lots of TiO_2 were found on the grain boundary of Mo-0.03Ti-A joint (the joint with the highest strength). The increase in strength might be a result of the change in the bonding strength of the grain boundaries caused by the difference in the precipitated phase on the grain-boundary surface. Therefore, it is necessary to analyse the state of the grain-boundary surface after alloying with Ti. In addition, in view of the significant increase in joint strength resulting from the use of method B for alloying, the metallurgical behaviour of the Ti foil pre-placed between the Mo tube and the Mo rod in the HAZ of the joint under thermal cycling is also discussed.

4.1. Distribution and existing forms of Ti on the grain-boundary surface in the weld bead

An XPS system that analyses the target zone within a very small depth range (approximately 0.5–3 nm for metallic materials) was used to analyse the composition of the grain-boundary surface in the weld bead zone of the Mo-0.03Ti-A joint. The binding energy of an element varies between different valences. The XPS spectrum of Ti on the grain-boundary surface subjected to peak separation and fitting treatments (Fig. 8(a)) shows that the existing forms of Ti included Ti $3p_{5/2}$ (8.08at%; binding energy: 454.1 eV [38]), Ti_2O_3 (19.09at%; binding energy: 459.1 eV [39]), TiO_2 (33.86at%; binding energy: 458.8 eV [38]) and high-valence Ti oxides Ti_xO_y (38.97at%; binding energy: 461.2–464.3 eV). The existing forms of Mo included Mo $3d_{5/2}$ (42.14at%) [40], Mo $3d_{3/2}$ (31.83at%) [40], MoO_xC_y (13.82at%; binding energy: 227.8 eV [40]) and MoO_2 (12.21at%; binding energy: 229.5 eV [41]) (Fig. 8(b)).

To further analyse the distribution characteristics of Ti and Mo near the grain boundaries in the depth direction, an Ar^+ ion beam was used to sputter the grain-boundary surface for 90 s; the peeling speed was set to 0.24 nm/s in the depth direction (using peeling speed of tantalum oxide as standard). A new surface 21.6 nm away from the grain-boundary surface was obtained. The existing forms of Ti on the new surface were the same as those on the grain-boundary surface, whereas the existing forms of Mo on the new surface changed to free Mo, MoO_2 and Mo_2C . There was also a certain difference in the relative elemental contents along the grain-boundary depth direction. The relative content of free Ti increased from 8.08at% on the grain-boundary surface to 12.17at% on the new surface, whereas the TiO_2 content decreased from 38.97at% to 13.43at% (Fig. 8(c)). The MoO_2 content also increased from 12.21at% to 16.56at% (Fig. 8(d)).

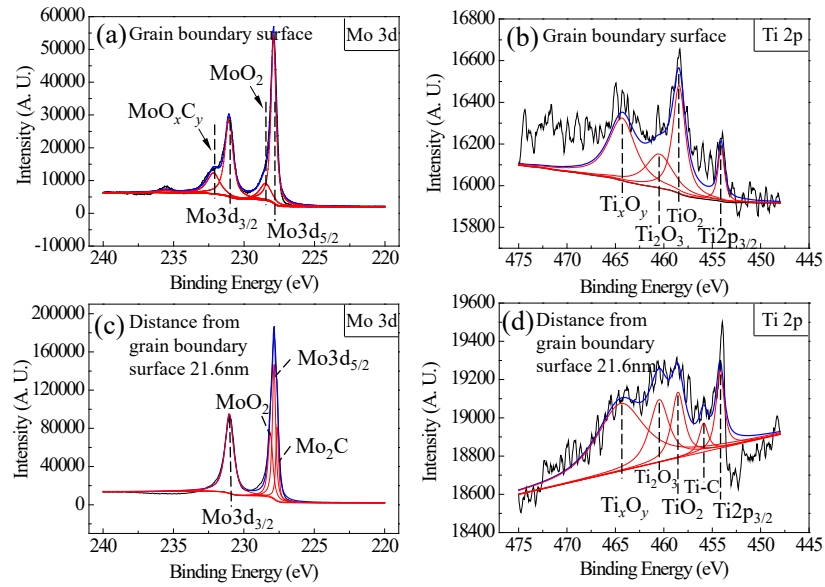


Fig. 8. XPS spectra of Mo 3d and Ti 2p on the grain-boundary and subgrain-boundary surfaces in the weld bead zone of the Mo-0.03Ti-A joint: (a) and (b): grain-boundary surface; (c) and (d): new surface 21.6 nm away from the grain-boundary surface

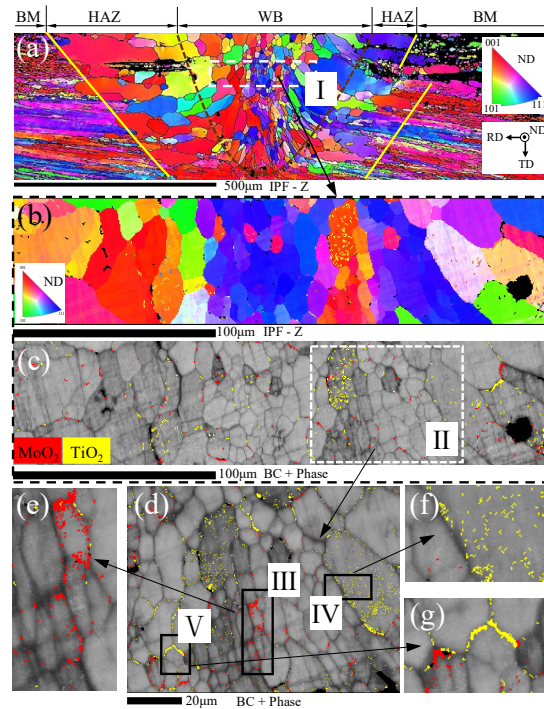


Fig. 9. EBSD cross-sectional analysis results for the welded zone of the Mo-0.03Ti-A joint.

The XPS measurements of the relative content of phase (Mo and Ti) were only semi-quantitative. Therefore, an EBSD system was used to further determine the relative content of each phase in the welded zone of the Mo-0.03Ti-A joint. The results in Table 3 show the following. The main phases in the weld bead zone of the Mo-0.03Ti-A joint were Mo, TiO_2 (relative content: 2.93% (the ratio of the count of the TiO_2 phase to the total count in EBSD)) and MoO_2 (relative content: 2.09%). The phases with a relatively high content (TiO_2 and MoO_2) exhibited a certain regular distribution pattern. As shown in Fig. 9(d), TiO_2 was distributed in the Mo grains (zone IV) or at the Mo grain boundaries (zone V) in a dotted or chain-like pattern, whereas MoO_2 was mainly distributed at the Mo grain boundaries (zone III) in a dotted or sheet-like pattern. In addition, the MoO_2 content decreased significantly in zones where a large amount of TiO_2 was distributed.

Table 2. EBSD results of relative contents of different phases in fusion zone shown in Fig. 9(a)

Phase	Mo	TiO ₂	Ti ₂ O ₃	MoO ₂	Mo ₂ C	Rate of no resolution
Phase percent (%)	84.55	2.93	0.57	2.09	0.38	9.48

5. Conclusions

The maximum tensile strength of a Mo laser welded joint could reach 64.5% of the strength of the base material after being alloyed with Ti. Metallurgical bonding in the brazing layer in the HAZ could allow the strength of the Ti-alloyed Mo laser welded joint to be the same as that of the base material. The main conclusions derived from this study are summarized as follows.

1. After a small amount of Ti was added, some FGZs appeared in the welded zone, and the number of low- Σ value CSL grain boundaries in the welded zone increased significantly.
2. O concentrated at the Mo grain boundaries in the welded zone, forming MoO₂, which significantly reduced the tensile strength of the Mo laser welded joint. Adding a small amount of Ti could thwart the weakening effect of the impurity element O on the strength of the Mo laser welded joint.
3. The Ti added to the welded zone interacted with O and Mo, thereby reducing the free O content of the welded zone and the MoO₂ content at the grain boundaries. In addition, TiO₂ particles were formed at the grain boundaries and inside the grains. At the Mo grain boundaries, the MoO₂ phase and free O (both would significantly weaken the strength of the Mo grain boundaries) were partially replaced by the TiO₂ phase (which has almost no significant effect on the strength of the Mo grain boundaries), thereby achieving the goal of strengthening the joint.

Acknowledgements

This work was supported by the National Natural Science Foundation of P. R. China (Grant No. 51775416), National Thousand Talents Program of P. R. China (Grant No. WQ2017610446). The authors would thank teachers at Instrument Analysis Center of Xi'an Jiaotong University for their assistance with XPS, SEM, EBSD and TEM analysis. Jinduicheng Molybdenum Group Co., LTD is thanked for providing the material.

References

- [1] J.B. Brosse, R. Fillit, M. Biscondi, Intrinsic intergranular brittleness of molybdenum, *Scripta Metallurgica* 15(6) (1981) 619-623.
- [2] T. Watanabe, S. Tsurekawa, The control of brittleness and development of desirable mechanical properties in polycrystalline systems by grain boundary engineering, *Acta Materialia* 47(15-16) (1999) 4171-4185.
- [3] M.K. Miller, E.A. Kenik, M.S. Mousa, K.F. Russell, A.J. Bryhan, Improvement in the ductility of molybdenum alloys due to grain boundary segregation, *Scripta Materialia* 46(4) (2002) 299-303.
- [4] M.K. Miller, A.J. Bryhan, Effect of Zr, B and C additions on the ductility of molybdenum, *Materials Science & Engineering A* 327(1) (2002) 80-83.
- [5] A.V. Krajnikov, F. Morito, V.N. Slyunyaev, Impurity-induced embrittlement of heat-affected zone in welded Mo-based alloys, *International Journal of Refractory Metals & Hard Materials* 15(5) (1997) 325-339.
- [6] D.L. K. Leitner (née Babinsky), W. Knabl, M. Eidenberger-Schober, K. Huber, A. Lorich, H. Clemens, V. Maier-Kiener, Grain boundary segregation engineering in as-sintered molybdenum for improved ductility, *Scripta Materialia* 156 (2018) 60-63.
- [7] A. Kumar, B.L. Eyre, Grain Boundary Segregation and Intergranular Fracture in Molybdenum, *Proceedings of the Royal Society of London* 370(1743) (1980) 431-458.
- [8] Y. Hiraoka, M. Okada, R. Watanabe, Effect of aging after carbon doping on the ductility of molybdenum, *Journal of The Less-Common Metals* 75(1) (1980) 31-42.
- [9] Y. Hiraoka, S. Yoshimura, K. Takebe, Low-temperature tensile behavior of powder-metallurgy Mo-Ti Alloys, *International Journal of Refractory Metals & Hard Materials* 12(4) (1993) 211-216.
- [10] N.N. Morgunova, A.V. Abramyan, N.I. Kazakova, Effect of rhenium on the brittle fracture threshold of molybdenum, *Metal Science and Heat Treatment* 29(6) (1987) 441-447.
- [11] K. Leitner, D. Scheiber, S. Jakob, S. Primig, H. Clemens, E. Povoden-Karadeniz, L. Romaner, How grain boundary chemistry controls the fracture mode of molybdenum, *Materials & Design* 142 (2018) 36-43.
- [12] C. Pöhl, J. Schatte, H. Leitner, Solid solution softening of polycrystalline molybdenum-hafnium alloys, *Journal of Alloys & Compounds* 576(29) (2013) 250-256.

- [13] L.E. Olds, G.W.P. Rengstorff, Effect of small amounts of alloying elements on the ductility of cast molybdenum, *JOM* 9(4) (1957) 468-471.
- [14] J. Fan, M. Lu, H. Cheng, J. Tian, B. Huang, Effect of alloying elements Ti, Zr on the property and microstructure of molybdenum, *International Journal of Refractory Metals & Hard Materials* 27(1) (2009) 78-82.
- [15] T. Inoue, Y. Hiraoka, E.I. Sakedai, M. Nagae, J. Takada, Hardening behavior of dilute Mo-Ti alloys by two-step heat-treatment, *International Journal of Refractory Metals & Hard Materials* 25(2) (2007) 138-143.
- [16] Y. Hiraoka, K. Imamura, T. Kadokura, Y. Yamamoto, Carbon diffusion behavior in molybdenum at relatively low temperatures, *Journal of Alloys & Compounds* 489(1) (2010) 42-46.
- [17] W.D. Klopp, W.R. Witzke, Mechanical properties of electron-beam-melted molybdenum and dilute Mo-Re alloys, *Metallurgical Transactions* 4(8) (1973) 2006-2008.
- [18] A. Hasegawa, K. Ueda, M. Satou, K. Abe, Neutron irradiation embrittlement of molybdenum rhenium alloys and their improvement by heat treatment, *Journal of Nuclear Materials* 258-263(4) (1998) 902-906.
- [19] L.J. Zhang, J.Y. Pei, L.L. Zhang, J. Long, J.X. Zhang, S.J. Na, Laser seal welding of end plug to thin-walled nanostructured high-strength molybdenum alloy cladding with a Zirconium interlayer, *Journal of Materials Processing Technology* (2018).
- [20] K.S. Hwang, H.S. Huang, Identification of the segregation layer and its effects on the activated sintering and ductility of Ni-doped molybdenum, *Acta Materialia* 51(13) (2003) 3915-3926. [https://doi.org/10.1016/S1359-6454\(03\)00216-7](https://doi.org/10.1016/S1359-6454(03)00216-7).
- [21] Y. Hiraoka, S. Yoshimura, K. Takebe, Effects of complex additions of Re or Ti with C on the strength and ductility of recrystallized molybdenum, *International Journal of Refractory Metals & Hard Materials* 12(5) (1994) 261-268.
- [22] ASM Handbook: Vol. 3, Alloy Phase Diagrams (Materials Park, OH: ASM International 1992).
- [23] S.H. Davis, *Theory of Solidification*, Cambridge University Press 2001.
- [24] B.V. Cockeram, The Fracture Toughness and Toughening Mechanism of Commercially Available Unalloyed Molybdenum and Oxide Dispersion Strengthened Molybdenum with an Equiaxed, Large Grain Structure, *Metallurgical & Materials Transactions A* 40(12) (2009) 2843.